Reaction Rates Estimation for the Endocytic Reception in Extracellular Vesicles-Mediated Communications

Mohammad Zoofaghari
Yazd University//Oslo University Hospital
Yazd, Iran
zoofaghari@gmail.com

Martin Damrath
Norw. Uni. of Science and Tech.
Trondheim, Norway
martin.damrath@ntnu.no

Hamid Khoshfekr Rudsari
Oslo University Hospital//University of Oslo
Oslo, Norway
h.k.rudsari@studmed.uio.no

Fabrizio Pappalardo
DIEEI, University of Catania
Catania, Italy
fabrizio.pappalardo@phd.unict.it

Mladen Veletić
Oslo University Hospital//Norw. Uni. of Science and Tech.
Oslo, Norway
mladen.veletic@ntnu.no

Ilangko Balasingham
Oslo University Hospital//Norw. Uni. of Science and Tech.
Oslo//Trondheim, Norway
ilangko.balasingham@ntnu.no

ABSTRACT

The extracellular vesicles (EVs) role in intercellular communication of transferring the cargoes of biomolecules such as proteins and nucleic acid between cells has been revealed recently. EV-mediated molecular communications (MC) is involved in targeted cells that receive EVs following the mechanisms of endocytosis. Such mechanisms comprise various processes of EV binding, internalization, and recycling that are characterized by specific factors of reaction. Accurate estimation of these factors is essential for the MC receiver assessment upon EV signaling. Here, we propose a fitting model to approximate the reaction rate parameters based on a suggested scenario corresponding to an experimental setup. The results of relative error for the estimated rates based on the simulated data are presented. The estimation method given in this paper can help future works on data analysis and minimizing the experimental resources.

CCS CONCEPTS

• **Applied computing** → **Computational biology**; **Health care information systems**; *Physical sciences and engineering*.

NANOCOM '22, October 5–7, 2022, Barcelona, Spain

ACM ISBN 978-1-4503-9867-1/22/10.
https://doi.org/10.1145/3558583.3558848

KEYWORDS

Molecular communications, extracellular vesicle, endocytosis, EV internalization, reaction rate estimation.

ACM Reference Format:
Mohammad Zoofaghari, Martin Damrath, Hamid Khoshfekr Rudsari, Fabrizio Pappalardo, Mladen Veletić, and Ilangko Balasingham. 2022. Reaction Rates Estimation for the Endocytic Reception in Extracellular Vesicles-Mediated Communications. In *The Ninth Annual ACM International Conference on Nanoscale Computing and Communication (NANOCOM '22), October 5–7, 2022, Barcelona, Spain.* ACM, New York, NY, USA, 6 pages. https://doi.org/10.1145/3558583.3558848

1 INTRODUCTION

In several billion years, cells adopted multiple strategies to be able to communicate with each other. This accurate process regulates complex organisms such as animals or plants thanks to the production of thousands of molecules of different nature (proteins, hormones, lipids, RNA, etc.) [23]. Next to the receptor and the lipophilic pathways [9, 12], that allows the transmission of a single input, there is the possibility to transmit many inputs into the same "packet" called vesicle [5].

We use the molecular communications (MC) paradigm to model inter- and intra-cellular communication using chemical signals such as extracellular vesicles (EVs) and closely scrutinize the underlying mechanisms in EV-mediated communications. The EVs that are propagating in the extracellular matrix might be degraded due to their interaction with the hindering cells or half-life. This would be characterized by a channel degradation rate in the communication link. Also, the conditions governing the medium boundaries e.g. in intra-cellular communication are determined by the EVs internalization and binding rates to the cell membrane [3]. These rates also specify the uptake mechanism at the receiver.

The EVs that are bound to the cell might be recycled into the environment through a backward reaction as well [27]. Furthermore, there are some *in vitro* and *in vivo* evidences [13, 22] that shown EVs are taken up by the same cells that are released from, which should be taken into the account for the release rate estimation.

All these issues necessitate estimating chemical reaction rates involved in EVs reception, as a prior step in EV-based MC. This also has applications in designing drug delivery systems for therapeutic reasons or optimizing experimental test-beds by providing initial results.

Data acquisition for the parameter estimation is usually based on *"in vivo"*, *"in vitro"* or *"in silico"* (i.e. computer simulations) [19, 25] experiments. There are also various strategies for the data analysis including Nano-Tracking Analysis (NTA) [26], Confocal Microscopy Imaging (CMI) [20], Scansion Electron Microscopy (SEM) and Transmission Electron Microscopy (TEM) [11]. NTA is just aimed at overall uptake estimation while the internalization and binding mechanism could be distinguished by CMI, SEM and TEM at the expense of performing several experiments and using more resources.

For the parameter estimation, Cock et al. proposed a stochastic model for a first-order chemical reaction using the maximum likelihood method [8]. The number of biomolecules involved in the chemical reaction is approximated by a Gaussian distribution. However, this work lacks the backward reaction due to the first-order assumption. Furthermore, the estimation of reaction rates is given by [16] upon an ill-posed inverse problem. This approach hardly satisfies the uniqueness and stability of the results specially for noisy acquired experimental data.

In this paper, we model the overall EVs uptake by a second-order chemical reaction. This model encompasses all the processes of EVs binding, internalization and recycling. It is expressed in terms of ordinary differential equations (ODEs) whose coefficients are estimated through a complex fitting function that we derive in the frequency domain. This model corresponds to an comparably simple experimental setup shown in Figure 1 that we discuss later in this paper. Since all the reaction rates are incorporated in this model, there is no need to exploit advanced techniques such as confocal microscopy imaging to evaluate internalization and binding process. All reaction rates can be estimated based on a single experiment, which eliminates the need for several more complex experiments that may be affected by changing conditions.

In the following, in Section 2, we first explain the biological background of EVs for our purpose. Also, we study the modeling for the chemical reaction of EVs and introduce a closed form function for the estimation of uptake rates. In Section 3, we give the simulation results and verify the closed form function through particle-based simulation (PBS) and finally, we conclude the paper in Section 4.

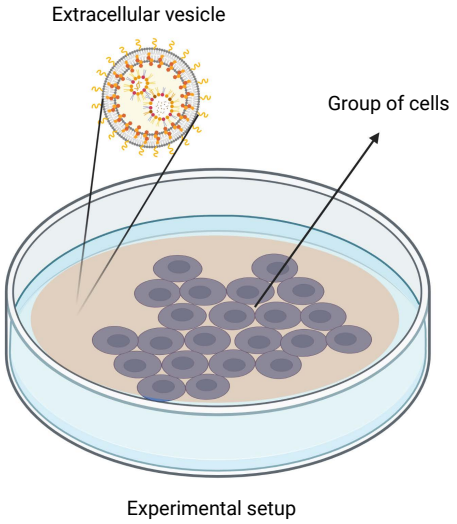

Figure 1: Experimental set-up of EVs reaction rates estimation. Isolated EVs are injected into the well in which the targeted cells are cultured and is filled in by the serum.

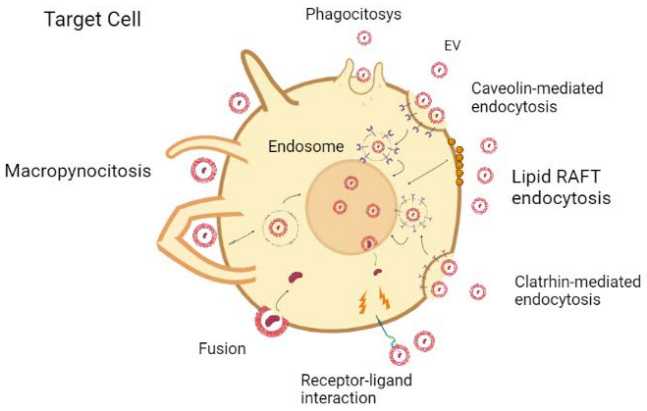

Figure 2: EVs Uptake. Vesicles are internalized by the target cell through many different pathways: endocytosis, fusion and juxtracine.

2 SYSTEM MODEL

EVs are generated by a "*donor cells*" in the Multi Vesicolar Body (MVB) and then are released into the extracellular fluid through the process of exocytosis and budding. They can also originate from recycling a group of vesicles internalized

before. As shown in Figure 1, the EVs in a well (dish of experiment) can be taken up through the different mechanisms by a group of cells cultivated at the bottom of the well. These mechanisms, shown in Figure 2, are studied in the literature as endocytosis (mediated with clathrin, caveoline and lipidic RAFT, pinocytosis [17] and fusion with the cell plasma membrane [18]. Ligand-binding (juxtracine pathway) can also take part in the reception process of EVs by the cells [14, 24]. Internalization of EVs might happen directly (e.g. through the fusion process) or after a stage of binding to the cell membrane.

As we discussed before, being aware of the chemical reaction rates on the cell membrane can help us to assess the channel response and receiver performance in a EV-mediated communication link. Here, we exploit a simplified reaction mechanism given by

$$\emptyset \xleftarrow{k_{\mathrm{h}}} \mathrm{A} \underset{k_{\mathrm{r}}}{\overset{k_{\mathrm{b}}}{\rightleftharpoons}} \mathrm{B} \xrightarrow{k_{\mathrm{i}}} \emptyset, \tag{1}$$

where 'A' and 'B' indicate the stimulating and bound EVs, respectively. In this model k_{b}, k_{i}, k_{r}, k_{h} denote binding, internalization, recycling and half-life rate of EVs, respectively. Some of these parameters may get zero value regarding to the type of endocytic mechanism. Endocytosis is influenced by the number of endocytosis sites on the cell surface. Here, we ignore the receptor saturation on the target cell for which all the binding spaces on the cell membrane are occupied. This is because the number of endocytosis sites is about 3000 in average per cell [21], while in this study we consider the number of initial EVs in the well by 1000.However, the model can be easily extended by taking receptor saturation into account. Please note that this model is just to apply to some of endocytosis mechanisms, which are already studied in the literature. [1, 7, 10, 21].

In order to estimate the reaction rates, we suggest a scenario of data acquisition as shown in Figure 1. In this setup, targeted cells which are to be evaluated for the uptake mechanism are cultivated at the bottom of a well which is filled in by q_0 number of stimulating EVs. This process can be done in parallel at several wells to get the remained number of EVs at different time samples. At first, EVs should be isolated from the wells through the several stages of filtration and centrifugation. Then, we need to characterize EVs by using NTA which can count the number of particles with varied sizes. NTA calculate the particles' hydrodynamic diameters based on Stokes Einstein equation and gives the size distribution of EVs. The serum that EVs are injected in, specifies the EVs half-life rate so k_{h} is assumed to be known (or obtained through another experiment).

Please note that we ignore the release of same EVs as those taken up by the target cells and exclude the release rate function in the formulation. However, EVs release could be incorporated through a separate experiment in which the cells are left in the EV-free wells and the number of generated EVs is specified over the time.

This uptake experiment is represented through a set of ODEs given by

$$\frac{\partial q_{\mathrm{B}}(t)}{\partial t} = k_{\mathrm{b}} q_{\mathrm{A}}(t) - k_{\mathrm{r}} q_{\mathrm{B}}(t) - k_{\mathrm{i}} q_{\mathrm{B}}(t), \tag{2}$$

$$\frac{\partial q_{\mathrm{A}}(t)}{\partial t} = -k_{\mathrm{b}} q_{\mathrm{A}}(t) + k_{\mathrm{r}} q_{\mathrm{B}}(t) - k_{\mathrm{h}} q_{\mathrm{A}}(t), \tag{3}$$

$$q_{\mathrm{A}}(0) = q_0, \quad q_{\mathrm{B}}(0) = 0, \tag{4}$$

where $q_{\mathrm{A}}(t)$ and $q_{\mathrm{B}}(t)$ stand for the number of EVs in the environment and the EVs bound to the cells, respectively. Reaction rates are estimated by measured $q_{\mathrm{A}}(t)$, through the model function derived from (2)-(4). In the cell-line experiment, EVs would be isolated from the wells at different time points and counted by NTA device to specify $q_{\mathrm{A}}(t)$ function. For now, we exploit the particle based simulation (PBS) to generate $q_{\mathrm{A}}(t)$ artificially. We remove the initial conditions given by (4) and insert the impulse function $q_0\delta(t)$ to the right-hand side of (3) and derive $q_A(t)$ by taking Fourier transform of (2) and (3) and solving the set of equations in frequency domain. After some simple manipulations, we have

$$\frac{q_0 - (j\omega + k_{\mathrm{h}})\tilde{q}_{\mathrm{A}}(j\omega)}{\tilde{q}_{\mathrm{A}}(j\omega)} = \frac{k_{\mathrm{b}}k_{\mathrm{i}} + k_{\mathrm{b}}j\omega}{k_{\mathrm{r}} + k_{\mathrm{i}} + j\omega}, \tag{5}$$

where $\tilde{q}_{\mathrm{A}}(j\omega)$ is the Fourier transform of $q_{\mathrm{A}}(t)$ at different angular frequency samples ω. It is observed in (5) that k_{b} is mainly dependent on the high frequency components of $\tilde{q}_{\mathrm{A}}(j\omega)$.

In order to estimate the rates coefficients k_{b}, k_{r}, and k_{i}, the number of environmental EVs over time, $q_{\mathrm{A}}(t)$, is transformed into the Fourier domain and the left-hand side of (5) over which the model function (i.e. the right-hand side) is fitted, would be obtained, where k_{b}, k_{r}, and k_{i} represent the non-negative fitting coefficients. The curve fitting can be solved, for example, by a nonlinear least-squares algorithm. It should be noted again that k_{h} is assumed to be known in this work, since half-life of EVs is a well-studied and easy to investigate issue. Nevertheless, k_{h} can also be determined by a reformulation of (5), although this will involve an overall rate estimate error increase.

Eqs. (2)-(4) can be exploited for various types and sizes of EVs for which different reaction rates would be obtained.

3 SIMULATION RESULTS

In this section we investigate the validity of the suggested model and the estimation error through numerical particle-based simulation. PBS results resemble the experimental data from the microscopic point of view. The curve fitting for parameter estimation is performed by the *MATLAB Optimization Toolbox*^{TM}, which uses a trust-region-reflective

Table 1: Default simulation parameters, which are applied throughout the numerical results, if not stated otherwise.

Parameters	Symbol	Value	Ref.
Binding rate	k_b	$2.3\ \mathrm{s}^{-1}$	[19]
Recycling rate	k_r	$0.11\ \mathrm{s}^{-1}$	[15]
Internalization rate	k_i	$0.005\ \mathrm{s}^{-1}$	[2]
Half-life rate	k_h	$3.85 \times 10^{-4}\ \mathrm{s}^{-1}$	[4]
Initial EV quantity	q_0	1000	
Time step in PBS	Δt	0.01 s	
Maximum time in PBS	T_max	1800 s	
PBS Monte Carlo runs	N	10^4	

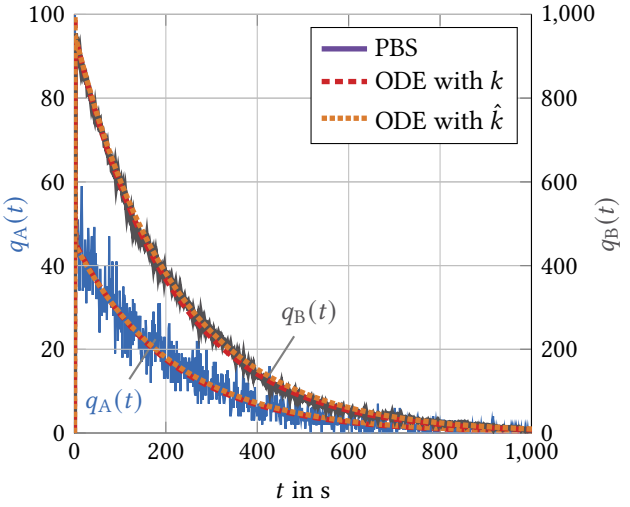

Figure 3: Obtained number of EVs in environment and bound to the cell with respect to time for a single PBS realization and ODE solution of (2) and (3). The considered parameters are given in Table 1.

method [6]. The simulation parameters and reference rate parameters under consideration are given in Table 1. Figure 3 shows $q_\mathrm{A}(t)$ and $q_\mathrm{B}(t)$ for a single realization of the PBS. As a comparison, the ODEs (2) and (3) are numerically solved as well, taking into account the reference rate parameters k, and the rate parameters $\hat{k}$ estimated by the PBS. It can be observed that the noisy PBS simulation follows the ODE solution. Furthermore, the ODE solution for $\hat{k}$ differs only slightly from the solution with k. From this, it can already be concluded that (5) leads to a good estimation, at least for the parameters under investigation. To have a precise assessment of the estimation results, the normalized mean

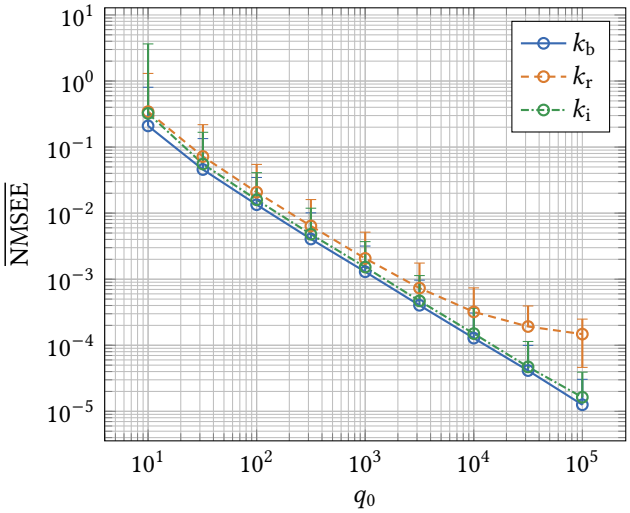

Figure 4: Normalized mean squared estimation error for the reaction rates with respect to initial number of EVs in the environment. The considered parameters are given in Table 1.

squared estimation error (NMSEE) is defined as

$$\overline{\mathrm{NMSEE}} = \frac{1}{N}\sum_{n=0}^{N-1}\left|\frac{k-\hat{k}}{k}\right|^2 . \tag{6}$$

Figure 4 shows the influence of the initial number of EVs q_0 in the environment on the NMSEE when estimating k_b, k_r and k_i. For all rates, the estimation improves with increasing q_0. This is to be expected, since the deviation from the expected value decreases with increasing number of EVs in PBS. In other words, the PBS result approaches the solution given in (2) and (3) as q_0 increases. Thus, Figure 4 also validates the proposed estimation approach according to (5). The estimation errors of k_b, k_r, and k_i are of the same order of magnitude in the considered scenario.

Number of initial EVs, q_0 might be overestimated or (as indicated in Figure 5 by $\hat{q}_0$) due to the limited accuracy of the NTA device. Figure 5 illustrates $\overline{\mathrm{NMSEE}}$ for the rate parameters versus the relative estimation error of q_0 in percent. As shown, for $q_0 = 10^3$, $\overline{\mathrm{NMSEE}}$ mainly changes for k_b and increases at most by 0.05 and 0.08 respectively, for 20% overestimation and underestimation of the initial EVs in the well. This demonstrates that the model is robust enough against q_0 variation. n each study, it is stated if other values are selected.

Figure 6 shows the effect of time step size Δt in PBS on rate estimation. While Δt for PBS can be chosen arbitrarily, the choice in laboratory measurements is limited by the available equipment and the total time required. Therefore it

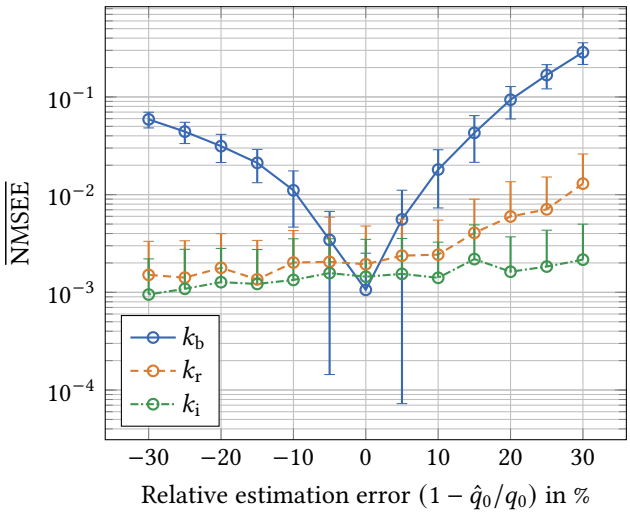

Figure 5: Normalized mean squared estimation error for the overestimation (negative relative estimation error) and underestimation (positive relative estimation error) of the number of initial EVs in the well.

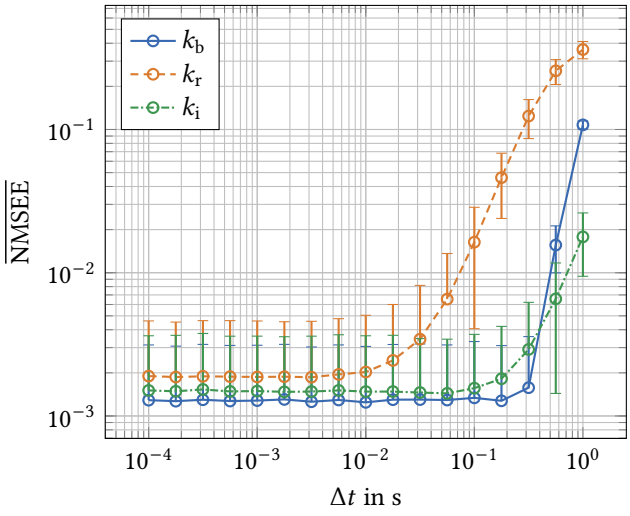

Figure 6: Normalized mean squared estimation error for the reaction rates with respect to time step size in PBS. The considered parameters are given in Table 1.

is interesting to investigate the influence of Δt on the parameter estimation, especially if Δt increases. As Δt increases, two effects cause the rate estimate to degrade. The first effect is that fewer samples are available for estimation according to (5), which worsens the fitting. A suitable interpolation between the measured values can reduce this effect. The second effect is that PBS results become imprecise with increasing step size due to very high reaction probabilities. It should

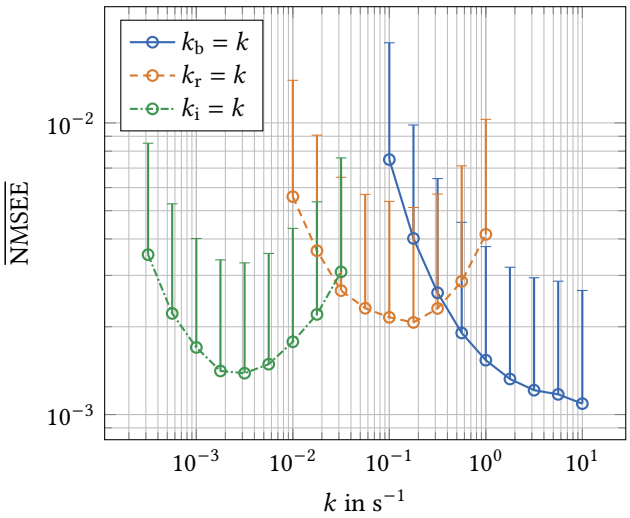

Figure 7: Normalized mean squared estimation error for the reaction rates with respect to reaction rate value. The considered parameters are given in Table 1.

be noted that this is only a problem of implementation of PBS and not of practical measurements. For the considered scenario, a significant degradation of the estimate starts from $\Delta t > 0.01$ s. A significant improvement of the estimate is not observed for $\Delta t < 0.01$ s.

Figure 7 shows the effect on the $\overline{\text{NMSEE}}$ of k_b, k_r, or k_i when these are varied, respectively. For this purpose, the rates were varied by a factor of 10 from their default value. The $\overline{\text{NMSEE}}$ is consistently low over the considered range. However, it can be seen that the rate value has an influence on the estimation error and the simulation parameters should be adjusted carefully. Larger reaction rates will, like an increase of Δt, lead to high reaction probabilities, which limits the accuracy of the PBS. Consequently, Δt should be decreased. For lower reaction rates, q_0 and the observation window given by T_max should be increased to acquire the entire reaction dynamics.

4 CONCLUSION

Chemical reactions of extracellular vesicles (EVs) with target cells are characterized in this paper by exploiting a suggested fitting model for the reaction rates estimation. The model is consistent with the various EVs endocytic mechanisms. The estimated parameters could be applied in channel modeling and receiver engineering in the framework of EV-mediated molecular communications. Simulation results demonstrated that the proposed fitting function provides less than 1% normalized mean squared estimation error for a wide range of reaction rates. However, the modeling of endocytosis can be improved by considering the saturation of receptors at

the target cell. The model is also well-adapted to the experimental setup introduced in this paper, which is supposed to be implemented in future work to minimize experimental resources and time-efficient data analysis. Nevertheless, the estimation method can be improved for a extended range of chemical reaction rate variations.

ACKNOWLEDGMENT

This work was supported in part by the Research Council of Norway under grant #287112 (RCN: CIRCLE Communication Theoretical Foundation of Wireless Nanonetworks).

REFERENCES

[1] Soheil Aghamohammadzadeh and Kathryn R Ayscough. 2009. Differential requirements for actin during yeast and mammalian endocytosis. *Nature cell biology* 11, 8 (2009), 1039–1042.

[2] Uma Thanigai Arasu, Kai Härkönen, Arto Koistinen, and Kirsi Rilla. 2019. Correlative light and electron microscopy is a powerful tool to study interactions of extracellular vesicles with recipient cells. *Experimental Cell Research* 376, 2 (2019), 149–158.

[3] Hamidreza Arjmandi, Mohammad Zoofaghari, and Adam Noel. 2019. Diffusive molecular communication in a biological spherical environment with partially absorbing boundary. *IEEE Transactions on Communications* 67, 10 (2019), 6858–6867.

[4] Chonlada Charoenviriyakul, Yuki Takahashi, Masaki Morishita, Akihiro Matsumoto, Makiya Nishikawa, and Yoshinobu Takakura. 2017. Cell type-specific and common characteristics of exosomes derived from mouse cell lines: Yield, physicochemical properties, and pharmacokinetics. *European Journal of Pharmaceutical Sciences* 96 (2017), 316–322.

[5] Emanuele Cocucci and Jacopo Meldolesi. 2015. Ectosomes and exosomes: shedding the confusion between extracellular vesicles. *Trends in cell biology* 25, 6 (2015), 364–372.

[6] Thomas F. Coleman and Yuying Li. 1996. An interior trust region approach for nonlinear minimization subject to bounds. *SIAM Journal on Optimization* 6, 2 (1996), 418–445.

[7] B áL Coomber and PA Stewart. 1985. Morphometric analysis of CNS microvascular endothelium. *Microvascular research* 30, 1 (1985), 99–115.

[8] Katrien De Cock, Xueying Zhang, Mónica F. Bugallo, and Petar M. Djurić. 2004. Stochastic simulation and parameter estimation of first order chemical reactions. In *2004 12th European Signal Processing Conference*. 1111–1114.

[9] Catherine Dostert, Melanie Grusdat, Elisabeth Letellier, and Dirk Brenner. 2019. The TNF family of ligands and receptors: communication modules in the immune system and beyond. *Physiological reviews* 99, 1 (2019), 115–160.

[10] Daisy Duan, Meretta Hanson, David O Holland, and Margaret E Johnson. 2022. Integrating protein copy numbers with interaction networks to quantify stoichiometry in clathrin-mediated endocytosis. *Scientific reports* 12, 1 (2022), 1–21.

[11] Peter J Goodhew, John Humphreys, and Richard Beanland. 2000. *Electron microscopy and analysis*. CRC press.

[12] MR Haussler, CA Haussler, PW Jurutka, PD Thompson, JC Hsieh, LS Remus, SH Selznick, and GK Whitfield. 1997. The vitamin D hormone and its nuclear receptor: molecular actions and disease states. *Journal of Endocrinology* 154, 3_Suppl (1997), S57–S73.

[13] Inbal Hazan-Halevy, Daniel Rosenblum, Shiri Weinstein, Osnat Bairey, Pia Raanani, and Dan Peer. 2015. Cell-specific uptake of mantle cell lymphoma-derived exosomes by malignant and non-malignant B-lymphocytes. *Cancer letters* 364, 1 (2015), 59–69.

[14] Guoku Hu, Lu Yang, Yu Cai, Fang Niu, Frank Mezzacappa, Shannon Callen, Howard S Fox, and Shilpa Buch. 2016. Emerging roles of extracellular vesicles in neurodegenerative disorders: focus on HIV-associated neurological complications. *Cell death & disease* 7, 11 (2016), e2481–e2481.

[15] Bongseop Kwak, Altug Ozcelikkale, Crystal S Shin, Kinam Park, and Bumsoo Han. 2014. Simulation of complex transport of nanoparticles around a tumor using tumor-microenvironment-on-chip. *Journal of Controlled Release* 194 (2014), 157–167.

[16] Adel Mhamdi and Wolfgang Marquardt. 1999. An inversion approach to the estimation of reaction rates in chemical reactors. In *1999 European Control Conference (ECC)*. IEEE, 3041–3046.

[17] EE Morrison, Matthew A Bailey, and JW Dear. 2016. Renal extracellular vesicles: from physiology to clinical application. *The Journal of physiology* 594, 20 (2016), 5735–5748.

[18] Laura Ann Mulcahy, Ryan Charles Pink, and David Raul Francisco Carter. 2014. Routes and mechanisms of extracellular vesicle uptake. *Journal of extracellular vesicles* 3, 1 (2014), 24641.

[19] Karin L Nicholson, Mary Munson, Rebecca B Miller, Thomas J Filip, Robert Fairman, and Frederick M Hughson. 1998. Regulation of SNARE complex assembly by an N-terminal domain of the t-SNARE Sso1p. *Nature structural biology* 5, 9 (1998), 793–802.

[20] Adaobi Nwaneshiudu, Christiane Kuschal, Fernanda H Sakamoto, R Rox Anderson, Kathryn Schwarzenberger, and Roger C Young. 2012. Introduction to confocal microscopy. *Journal of Investigative Dermatology* 132, 12 (2012), 1–5.

[21] Andrea Picco, Markus Mund, Jonas Ries, François Nédélec, and Marko Kaksonen. 2015. Visualizing the functional architecture of the endocytic machinery. *Elife* 4 (2015), e04535.

[22] María Sancho-Albero, Nuria Navascués, Gracia Mendoza, Víctor Sebastián, Manuel Arruebo, Pilar Martín-Duque, and Jesús Santamaría. 2019. Exosome origin determines cell targeting and the transfer of therapeutic nanoparticles towards target cells. *Journal of nanobiotechnology* 17, 1 (2019), 1–13.

[23] Dennis K Stone. 1998. Receptors: structure and function. *The American journal of medicine* 105, 3 (1998), 244–250.

[24] Saray Tabak, Sofia Schreiber-Avissar, and Elie Beit-Yannai. 2021. Influence of anti-glaucoma drugs on uptake of extracellular vesicles by trabecular meshwork cells. *International Journal of Nanomedicine* 16 (2021), 1067.

[25] Sandro Vivona, Daniel J Cipriano, Seán O'Leary, Ye Henry Li, Timothy D Fenn, and Axel T Brunger. 2013. Disassembly of all SNARE complexes by N-ethylmaleimide-sensitive factor (NSF) is initiated by a conserved 1: 1 interaction between α-soluble NSF attachment protein (SNAP) and SNARE complex. *Journal of Biological Chemistry* 288, 34 (2013), 24984–24991.

[26] John G Walker. 2012. Improved nano-particle tracking analysis. *Measurement Science and Technology* 23, 6 (2012), 065605.

[27] Mohammad Zoofaghari, Ali Etemadi, Hamidreza Arjmandi, and Ilangko Balasingham. 2021. Modeling Molecular Communication Channel in the Biological Sphere With Arbitrary Homogeneous Boundary Conditions. *IEEE Wireless Communications Letters* 10, 12 (2021), 2786–2790.